ALZHEIMER'S DISEASE

The BACE1 inhibitor verubecestat (MK-8931) reduces CNS β-amyloid in animal models and in Alzheimer's disease patients

Matthew E. Kennedy,[1]* Andrew W. Stamford,[2]* Xia Chen,[1] Kathleen Cox,[3] Jared N. Cumming,[2] Marissa F. Dockendorf,[3] Michael Egan,[4] Larry Ereshefsky,[5] Robert A. Hodgson,[1†] Lynn A. Hyde,[1] Stanford Jhee,[5] Huub J. Kleijn,[3‡] Reshma Kuvelkar,[1] Wei Li,[2] Britta A. Mattson,[6] Hong Mei,[3] John Palcza,[7] Jack D. Scott,[2] Michael Tanen,[8] Matthew D. Troyer,[9§] Jack L. Tseng,[9¶] Julie A. Stone,[3] Eric M. Parker,[1]* Mark S. Forman[9]*

β-Amyloid (Aβ) peptides are thought to be critically involved in the etiology of Alzheimer's disease (AD). The aspartyl protease β-site amyloid precursor protein cleaving enzyme 1 (BACE1) is required for the production of Aβ, and BACE1 inhibition is thus an attractive target for the treatment of AD. We show that verubecestat (MK-8931) is a potent, selective, structurally unique BACE1 inhibitor that reduced plasma, cerebrospinal fluid (CSF), and brain concentrations of Aβ40, Aβ42, and sAPPβ (a direct product of BACE1 enzymatic activity) after acute and chronic administration to rats and monkeys. Chronic treatment of rats and monkeys with verubecestat achieved exposures >40-fold higher than those being tested in clinical trials in AD patients yet did not elicit many of the adverse effects previously attributed to BACE inhibition, such as reduced nerve myelination, neurodegeneration, altered glucose homeostasis, or hepatotoxicity. Fur hypopigmentation was observed in rabbits and mice but not in monkeys. Single and multiple doses were generally well tolerated and produced reductions in Aβ40, Aβ42, and sAPPβ in the CSF of both healthy human subjects and AD patients. The human data were fit to an amyloid pathway model that provided insight into the Aβ pools affected by BACE1 inhibition and guided the choice of doses for subsequent clinical trials.

INTRODUCTION

The brains of patients with Alzheimer's disease (AD) are characterized by two histopathological hallmarks, namely, extracellular amyloid plaques largely composed of the β-amyloid (Aβ) peptides and intraneuronal neurofibrillary tangles composed primarily of hyperphosphorylated tau protein (*1*). The amyloid hypothesis of AD proposes that aberrant production and/or clearance of Aβ, principally aggregated species of Aβ in the form of soluble oligomers and insoluble plaques, triggers the underlying disease pathogenesis that ultimately leads to neuronal cell death and cognitive decline (*2*). Aβ is formed via sequential cleavage of the amyloid precursor protein (APP) by the aspartyl proteases β-site amyloid precursor protein cleaving enzyme 1 (BACE1 or β-secretase) (*3*) and γ-secretase. BACE1 cleavage of APP produces a secreted N-terminal fragment known as soluble amyloid precursor protein β (sAPPβ) and a C-terminal integral membrane protein fragment known as C99. The subsequent heterogeneous processing of C99 by γ-secretase produces a family of Aβ peptides, some of which (most notably Aβ42) are prone to aggregate into toxic species (*4*).

In addition to the fact that the pathognomonic amyloid plaques are composed largely of Aβ, the amyloid hypothesis is supported by a compelling body of genetic, biochemical, and imaging evidence (*5*). Familial AD mutations in APP or in the γ-secretase components presenilin-1 and presenilin-2 increase the production and/or aggregation potential of Aβ. Duplication or triplication of the APP gene (for example, as occurs in Down syndrome) is also associated with increased Aβ production, early onset amyloid deposition, and dementia. The *APOE4* allele, the most common genetic risk factor for sporadic AD, is also known to increase the rate and/or extent of amyloid deposition in mouse models and in humans. Finally, amyloid deposition in the brain and decreased concentration of Aβ42 in the cerebrospinal fluid (CSF) are associated with frank dementia or cognitive impairment or with a higher risk of progressing to dementia/cognitive impairment.

Given the strong evidence supporting the amyloid hypothesis, research has focused on the development of amyloid-lowering therapies for the treatment of AD, with BACE1 inhibition being one of the most attractive approaches (*3*). Genetic deletion of BACE1 eliminates Aβ production and resolves the amyloid plaques and cognitive/behavioral deficits observed in transgenic mice overexpressing human APP with familial AD mutations (*6*–*8*). Furthermore, a rare human mutation at the BACE1 cleavage site of APP has been identified, which results in a 40% decrease in Aβ production in vitro, a reduced propensity of Aβ to aggregate, a five- to sevenfold reduced risk of developing AD, and improved cognitive function in elderly subjects without AD (*9*–*11*). Despite major research programs in industry and academia prompted by these strong supporting data, efforts to design and develop selective, cell-permeable, orally bioavailable, brain-penetrant BACE1 inhibitors have proved extremely challenging (*3*). Recent genetic deletion and pharmacological inhibition studies, the identification of new BACE1 substrates, and the detection of potentially toxic Aβ species modulated by BACE1 have also suggested possible adverse consequences of BACE1

[1]Department of Neuroscience, Merck Research Laboratories, Kenilworth, NJ 07033, USA. [2]Department of Global Chemistry, Merck Research Laboratories, Kenilworth, NJ 07033, USA. [3]Department of Pharmacokinetics, Pharmacodynamics and Drug Metabolism, Merck Research Laboratories, Kenilworth, NJ 07033, USA. [4]Department of Clinical Research, Merck Research Laboratories, Kenilworth, NJ 07033, USA. [5]PAREXEL, Glendale, CA 91206, USA. [6]Department of Safety Assessment, Merck Research Laboratories, West Point, PA 19446, USA. [7]Department of Biostatistics, Merck Research Laboratories, Kenilworth, NJ 07033, USA. [8]Translational Biomarkers Department, Merck Research Laboratories, Kenilworth, NJ 07033, USA. [9]Department of Translational Medicine, Merck Research Laboratories, Kenilworth, NJ 07033, USA.
*Corresponding author. Email: matthew.kennedy@merck.com (M.E.K.); andy.stamford1@gmail.com (A.W.S.); ericmcparker@comcast.net (E.M.P.); mark.forman@merck.com (M.S.F.)
†Present address: Charles River Laboratories, Wilmington, MA 01887, USA.
‡Present address: Quantitative Solutions, Oss, Netherlands.
§Present address: Medivation, San Francisco, CA 94105, USA.
¶Present address: Purdue Pharma, Stamford, CT 06901, USA.

inhibition [for a review, see (*12*)]. Finally, the lack of clinical benefit in previous trials of amyloid-lowering agents has been cited as evidence against the amyloid hypothesis and against additional testing of these agents (*2*, *5*). We report here on the discovery and characterization of verubecestat (MK-8931), the first BACE1 inhibitor to progress to phase 3 clinical trials in AD patients and currently the agent best positioned to provide a definitive test of both the amyloid hypothesis and the safety and efficacy profile of BACE1 inhibition in AD patients.

RESULTS

Discovery of verubecestat

To overcome the many challenges inherent in identifying BACE1 inhibitors (*3*, *13*), fragment screening by nuclear magnetic resonance was used to identify structurally unique, active site–directed, nonpeptidomimetic leads that could be optimized into BACE1 inhibitors with central nervous system (CNS) drug–like properties (*13*). This screening effort identified isothiourea 1 as a weak BACE1 ligand (Fig. 1A), and an x-ray cocrystal structure of this compound bound to BACE1 revealed that its amidine moiety engages in an unprecedented hydrogen bond donor-acceptor network with the BACE1 catalytic dyad of Asp^{32} and Asp^{228} (Fig. 1B) (*13*). Through application of structure-based design, medicinal chemistry optimization, and early in vivo screening, isothiourea 1 was developed into a new, nonpeptidic class of BACE1 inhibitors, an effort that culminated in the discovery of verubecestat {*N*-[3-[(5*R*)-3-amino-5,6-dihydro-2,5-dimethyl-1,1-dioxido-2*H*-1,2,4-thiadiazin-5-yl]-4-fluorophenyl]-5-fluoro-2-pyridinecarboxamide} (Fig. 1C) (*13*). An x-ray cocrystal structure confirmed hydrogen bonding interactions between the amidine moiety of verubecestat and the BACE1 catalytic dyad (Fig. 1D). The diaryl amide substituent occupies the contiguous, relatively hydrophobic S1, S3, and $S3^{sp}$ subsites of BACE1, contributing to its high-affinity binding (Fig. 1D). Verubecestat has physicochemical properties that are highly favorable for an orally absorbed, brain-penetrant drug, including high cellular permeability ($P_{app} = 28.6 \times 10^{-6}$ cm•s^{-1}) and high aqueous solubility at neutral pH (1.6 mM in pH 7.4 buffer).

In vitro activity of verubecestat

Verubecestat is a potent inhibitor of purified human and mouse Bace1 [inhibition constant (K_i) = 2.2 and 3.4 nM, respectively] and also inhibits Aβ40, Aβ42, and sAPPβ production in human cells with similar potency [median inhibitory concentration (IC_{50}) = 2.1, 0.7, and 4.4 nM, respectively; Table 1]. The compound is also a potent inhibitor of purified human BACE2 (K_i = 0.38 nM; Table 1), a structurally related aspartyl protease (*3*). Verubecestat is essentially inactive in the purified human aspartyl proteases cathepsin D (CatD), cathepsin E (CatE), and pepsin (>45,000-fold selectivity) and is a very weak inhibitor of purified human renin (15,000-fold selectivity; Table 1). Verubecestat also has minimal or no activity against a large panel of receptors, ion channels, transporters, and enzymes (table S1). The compound weakly inhibits the human Ether-A-Go-Go (hERG) channel (IC_{50} = 2.2 μM).

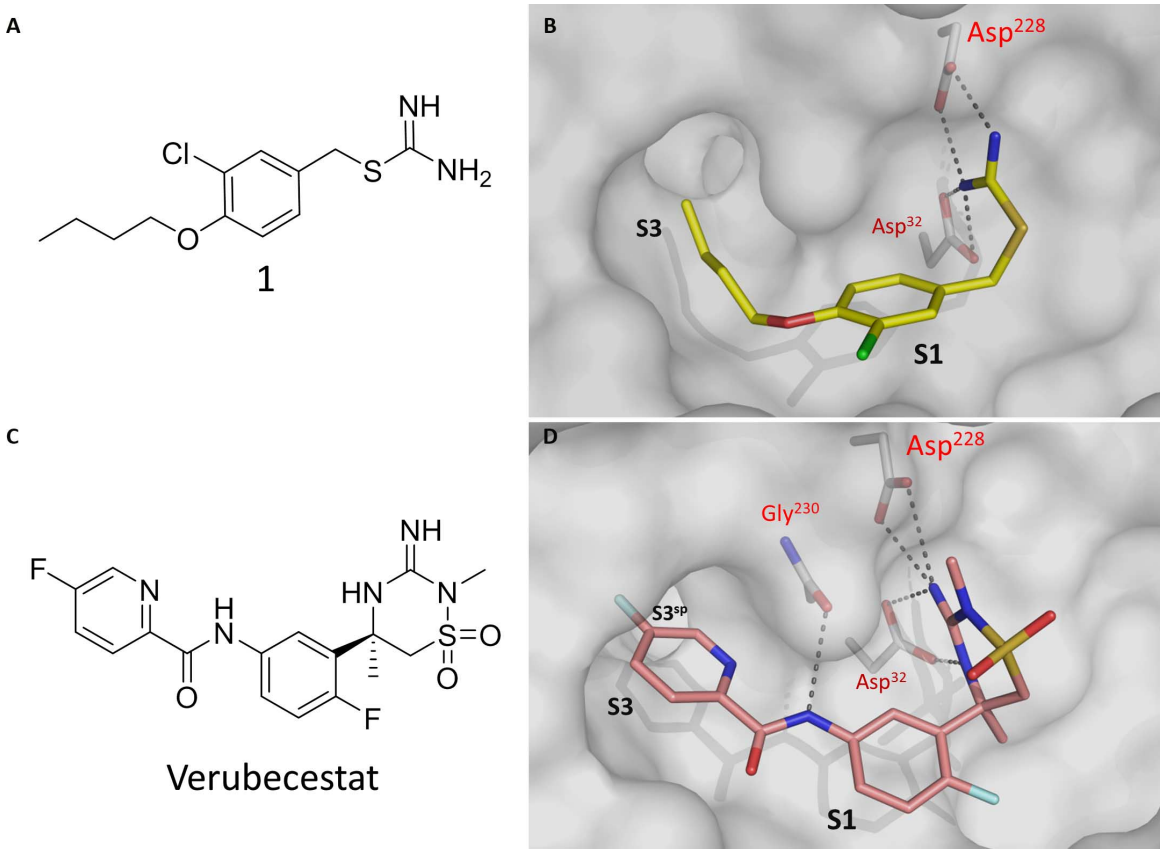

Fig. 1. Discovery of verubecestat from a weakly active fragment lead using structure-based drug design. X-ray crystallography of the isothiourea fragment lead 1 (**A**) and verubecestat (**C**) bound to the human BACE1 soluble enzymatic domain were carried out as described (*41*). The x-ray cocrystal structure of the fragment lead 1 bound to the active site of human BACE1 determined at 1.8 Å resolution is shown in (**B**). Verubecestat bound to the active site of human BACE1 determined at 1.74 Å resolution is shown in (**D**). Hydrogen bonds are indicated by the dashed lines. S1, subsite 1; S3, subsite 3; $S3^{sp}$, subsite 3 subpocket.

Table 1. Potency of verubecestat to inhibit BACE1 and other human aspartyl proteases. Data are means ± SD of results from two to five independent experiments performed in duplicate. h, human; m, mouse; HEK293, human embryonic kidney–293.

Enzyme or cell line	Verubecestat K_i or IC_{50} (nM)
hBACE1	2.2 ± 1.4
mBACE1	3.4 ± 0.68
hBACE2	0.38 ± 0.37
hCatD	>>100,000
hCatE	>>100,000
hPepsin	>>100,000
hRenin	33,800 ± 12,640
HEK293 Aβ40	2.1 ± 1.8
HEK293 Aβ42	0.7 ± 0.09
HEK293 sAPPβ	4.4 ± 1.4

In vivo activity of verubecestat

After administration of a single oral dose of 10 or 30 mg/kg to rats, verubecestat reduced CSF and cortical Aβ40 substantially, with the peak effects occurring 3 to 6 hours after dosing (Fig. 2, A and B). The peak reduction of CSF and cortical Aβ40 was delayed relative to the peak concentrations of verubecestat in plasma, brain, and CSF, which were observed ≤1 hour after dosing (fig. S1). This delay is consistent with previous studies [for example, (*14*)] and is likely attributable to multiple factors, for example, the time required for metabolism and transport of preexisting Aβ.

Single oral doses of verubecestat in rats produced dose-dependent reductions in plasma, CSF, and cortical Aβ40 3 hours after administration, the time of the peak effect defined above (Fig. 2, C and D). The half-maximal effective dose values for reduction of plasma, CSF, and cortical Aβ40 were 0.03, 5, and 8 mg/kg, respectively (Fig. 2C), whereas the total (free) plasma median effective concentration values were ~3 (~1.1), 130 (48), and 220 (81) nM, respectively (Fig. 2D and table S2). Maximal Aβ40 reductions of >90% were achieved in all three compartments (Fig. 2, C and D). The CSF/unbound plasma concentration ratio in rats was below the theoretical value of 1, consistent with the observation that verubecestat is a substrate of the P-glycoprotein efflux transporter (BA/AB transport ratio = 11 in LLC-PK1 cells expressing human MDR1) (*15*). These values were 0.020 to 0.025 in the rat time course study shown in Fig. 2 (A and B) (see fig. S1) but were much higher (0.24 to 0.89) in the rat dose-response study shown in Fig. 2 (C and D) (see table S2). The reason for this discrepancy is not known.

In a time course study in cynomolgus monkeys, single oral doses of verubecestat (3 and 10 mg/kg) significantly reduced concentrations of CSF Aβ40 and sAPPβ (Fig. 3A and fig. S2). By 12 to 24 hours after dosing, CSF Aβ40 and sAPPβ were maximally reduced by 72% [$P < 0.02$ versus baseline and $P < 0.001$ versus vehicle, analysis of variance (ANOVA)] and 71% ($P < 0.003$ versus baseline and $P < 0.0002$ versus vehicle, ANOVA), respectively, at 3 mg/kg and by 81% ($P < 0.02$ versus baseline and $P < 0.01$ versus vehicle, ANOVA) and 65% ($P < 0.0001$ versus baseline and $P < 0.0009$ versus vehicle, ANOVA), respectively, at 10 mg/kg. As reported previously, the maximum reduction in CSF sAPPβ was delayed relative to CSF Aβ40 (*16*), probably due to the slower turnover of sAPPβ. The inhibitory effect of verubecestat on CSF Aβ40 and sAPPβ was sustained at close to maximal levels for 24 hours, which was consistent with CSF concentrations being maintained at or above the cell IC_{50} for Aβ40 reduction (Fig. 3B). In a separate study in cynomolgus monkeys, verubecestat reduced CSF and cortical Aβ40 by 60% ($P < 0.05$ versus baseline CSF, *t* test) and 72% ($P < 0.05$ versus control cortex, *t* test), respectively, 4 hours after a single oral dose of 10 mg/kg (Fig. 3C). The reduction in CSF Aβ40 was similar in magnitude to that seen in the continuous CSF sampling studies (compare Fig. 3, A and C). The CSF/unbound plasma concentration ratio of verubecestat in the monkey studies reported here ranged from 0.12 to 0.56 (Fig. 3B and tables S3 and S4).

The acute reduction of CSF and cortical Aβ40 produced by verubecestat was maintained after chronic administration. Once-daily oral administration of verubecestat (10, 30, or 100 mg/kg) to cynomolgus monkeys for 9 months produced substantial (>80%) reduction of CSF Aβ40, Aβ42, and sAPPβ as well as cortical Aβ40 and sAPPβ (fig. S3), consistent with results from acute studies (compare Fig. 3). The ability of verubecestat to markedly reduce cortical Aβ40 was also maintained after chronic administration to rats for 3 months (fig. S4 and table S5).

Verubecestat demonstrated favorable pharmacokinetic (PK) properties in multiple animal species, including high oral bioavailability and exposure, modest protein binding, and a reasonable half-life ($t_{1/2}$) (table S6). Allometric scaling of the animal PK data predicted that verubecestat would have an effective human $t_{1/2}$ of ~11 hours and a high oral bioavailability (*F*) of ~75%. A low daily oral dose of ~35 mg and a relatively modest total plasma C_{max} and area under the curve at 0- to 24-hour [$AUC_{(0–24\ hr)}$] values (218 nM and 2.35 μM*hour, respectively) were projected to produce the targeted 75% inhibition of CSF Aβ40 at steady state.

Safety of chronic verubecestat treatment in animals

Constitutive Bace1 knockout mice have been reported to have a reduction in central and peripheral nerve myelination (*3*, *12*, *17*, *18*), whereas constitutive Bace2 knockout mice have been reported to have reduced blood glucose, increased pancreatic β cell mass, and fur hypopigmentation (*19*–*21*). Furthermore, BACE inhibitors have been shown to cause neurodegeneration, fur hypopigmentation, increased pancreatic β cell mass, reduced blood glucose, and/or hepatotoxicity in animals or in humans (*14*, *19*–*22*). Therefore, chronic toxicology studies of verubecestat in rats (0, 5, 25, or 75 mg kg^{-1} day^{-1} for 6 months) and monkeys (0, 10, 30, or 100 mg kg^{-1} day^{-1} for 9 months) included evaluations that probed whether verubecestat induces these BACE-associated adverse effects. Near-maximal inhibition of BACE1 was confirmed by nearly complete reductions in CSF and cortical Aβ40, Aβ42, and sAPPβ at all doses [up to 95% in monkeys (fig. S3); not determined in this rat study, but substantial reductions were likely achieved on the basis of reductions observed after treatment of rats with verubecestat for 3 months (fig. S4)]. At the highest dose tested in rats (75 mg kg^{-1} day^{-1}) and monkeys (100 mg kg^{-1} day^{-1}), the systemic exposures were 43- and 54-fold greater, respectively, than the systemic exposure achieved in humans at the highest dose being tested in phase 3 clinical trials (40 mg, see below). In rats and monkeys treated chronically with verubecestat, there were no antemortem behavioral observations, clinical signs, or clinical chemistry changes attributable to neurodegeneration or hepatotoxicity, as well as no effects on serum glucose (tables S7 and S8). Likewise, there were no postmortem findings consistent with histomorphologic or myelination changes in sciatic nerve or brain, neurodegeneration in

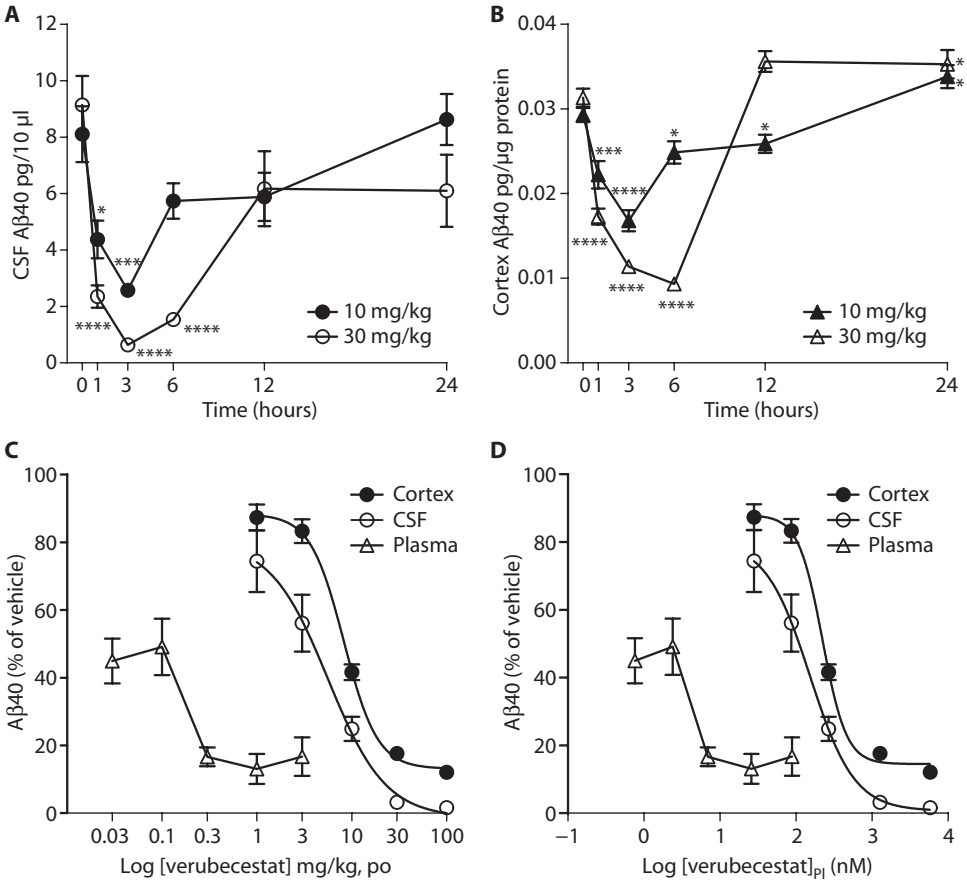

Fig. 2. Oral administration of verubecestat in rats. Acute oral administration of verubecestat in rats produced time-dependent and dose-dependent reductions in plasma, CSF, and cortical Aβ40. Time course profiles for CSF (**A**) and cortex (**B**) Aβ40 concentrations in Sprague-Dawley rats (n = 8 to 16 per group) orally administered vehicle or a single dose of verubecestat (10 or 30 mg/kg). Blood, CSF, and cortex were collected from separate groups of animals harvested at 0 (vehicle), 1, 3, 6, 12, and 24 hours after dosing with verubecestat. (**C**) Acute dose response for verubecestat-mediated reduction of plasma, CSF, and cortex Aβ1–40 concentrations in Sprague-Dawley rats (n = 8) normalized to Aβ40 concentrations in vehicle-treated animals. (**D**) Normalized Aβ40 data from (C) plotted versus total plasma concentrations of verubecestat at 3 hours after dosing. Data shown in (A) to (D) are means ± SEM. For (A) and (B), *P < 0.05, ***P < 0.001, ****P < 0.0001 as determined by Dunnett's multiple comparison test (GraphPad Prism). Concentrations of endogenous rat Aβ1–40 were determined by immunoassay (*40*). Plasma, CSF, and brain concentrations of verubecestat from this study are shown in fig. S1 and table S2.

the central or peripheral nervous systems, histomorphologic changes in pancreatic β cells, or hepatotoxicity. As recently reported with another BACE inhibitor (*20*), hypopigmentation of hair was observed in pigmented mice and rabbits treated with verubecestat (fig. S5; pigmentation changes could not be assessed in albino rats treated for 6 months with verubecestat). In rabbits treated with verubecestat, patches of black fur turned to a silver-gray color starting about 2 to 3 weeks after the initiation of dosing. The area of silver-gray fur increased with continued treatment with verubecestat. There was no evidence for hypopigmentation in the eye, nor was there any evidence of changes in skin architecture except for the lack of pigment in the hair follicles (fig. S5). Furthermore, no pigment changes were observed in any tissue in monkeys treated for 9 months with verubecestat.

Verubecestat reduces CSF Aβ and sAPPβ in healthy adults and AD patients

Having established the promising preclinical profile of verubecestat, human testing of the compound was initiated. Initially, single ascending doses of verubecestat were examined relative to placebo in healthy nonelderly adults. After placebo administration, CSF concentrations of Aβ40, Aβ42, and sAPPβ increased over the 36-hour sampling period (Fig. 4), a phenomenon that has been observed in previous human studies using serial CSF sampling [for example, (*23*)]. All doses of verubecestat produced maximal reduction in plasma Aβ40 (fig. S6). Time-weighted average 12- to 24-hour [$TWA_{(12–24\ hr)}$] CSF Aβ40 reductions of 41, 59, and 76% and maximal CSF Aβ40 reductions of 48, 77, and 93% were observed at the 20-, 100-, and 550-mg doses, respectively (Fig. 4). The magnitude and time course of reduction of CSF Aβ40, Aβ42, and sAPPβ were very similar at each dose, and, as observed in animals (see above), the maximal effects were delayed relative to the PK T_{max} (compare Fig. 4 and table S9). As observed in monkeys and as reported previously (*16*), the maximum reduction of CSF sAPPβ was delayed relative to CSF Aβ40 and Aβ42.

Subsequently, multiple ascending doses of verubecestat were examined relative to placebo in healthy nonelderly adults. Plasma Aβ40 was again maximally reduced at doses ≥40 mg (fig. S7). $TWA_{(0–24\ hr)}$ CSF Aβ40 reductions of 44, 83, 92, and 94% and maximal CSF Aβ40 reductions of 66, 87, 94, and 95% were observed at the 10-, 40-, 150-, and 250-mg doses, respectively [Fig. 5; note that these pharmacodynamic (PD) markers of BACE1 activity were not measured in the 80-mg dose group]. As seen in the single-dose studies, the magnitude and time course of reduction of CSF Aβ40, Aβ42, and sAPPβ were similar at each dose.

Verubecestat was then tested in mild to moderate AD patients to understand how the presence of disease might alter the safety, tolerability, PK, and the PD response of CSF Aβ and sAPPβ. $TWA_{(0–24\ hr)}$ CSF Aβ40 reductions of 57, 79, and 84% and maximal CSF Aβ40 reductions of 70, 83, and 90% were observed at the 12-, 40-, and 60-mg doses, respectively (Fig. 6). The magnitude and time course of these reductions were similar to those observed in healthy subjects (compare Figs. 5 and 6). As in the studies in healthy nonelderly adults, the magnitude and time course of reductions in Aβ42 and sAPPβ were similar to those for Aβ40.

Verubecestat displayed consistent, well-behaved PK properties across all three human studies. There was a near dose-proportional increase in exposure in both CSF and plasma, and concentrations in both compartments declined monoexponentially with similar rates of elimination (effective plasma half-life of ~14 to 24 hours), indicating rapid attainment of a dynamic equilibrium between the plasma and CSF compartments (tables S9 to S11). The geometric mean CSF/unbound plasma concentration ratio ranged from 0.1 to 0.6 across the various studies and time points. Moderate accumulation was observed after multiple daily dosing

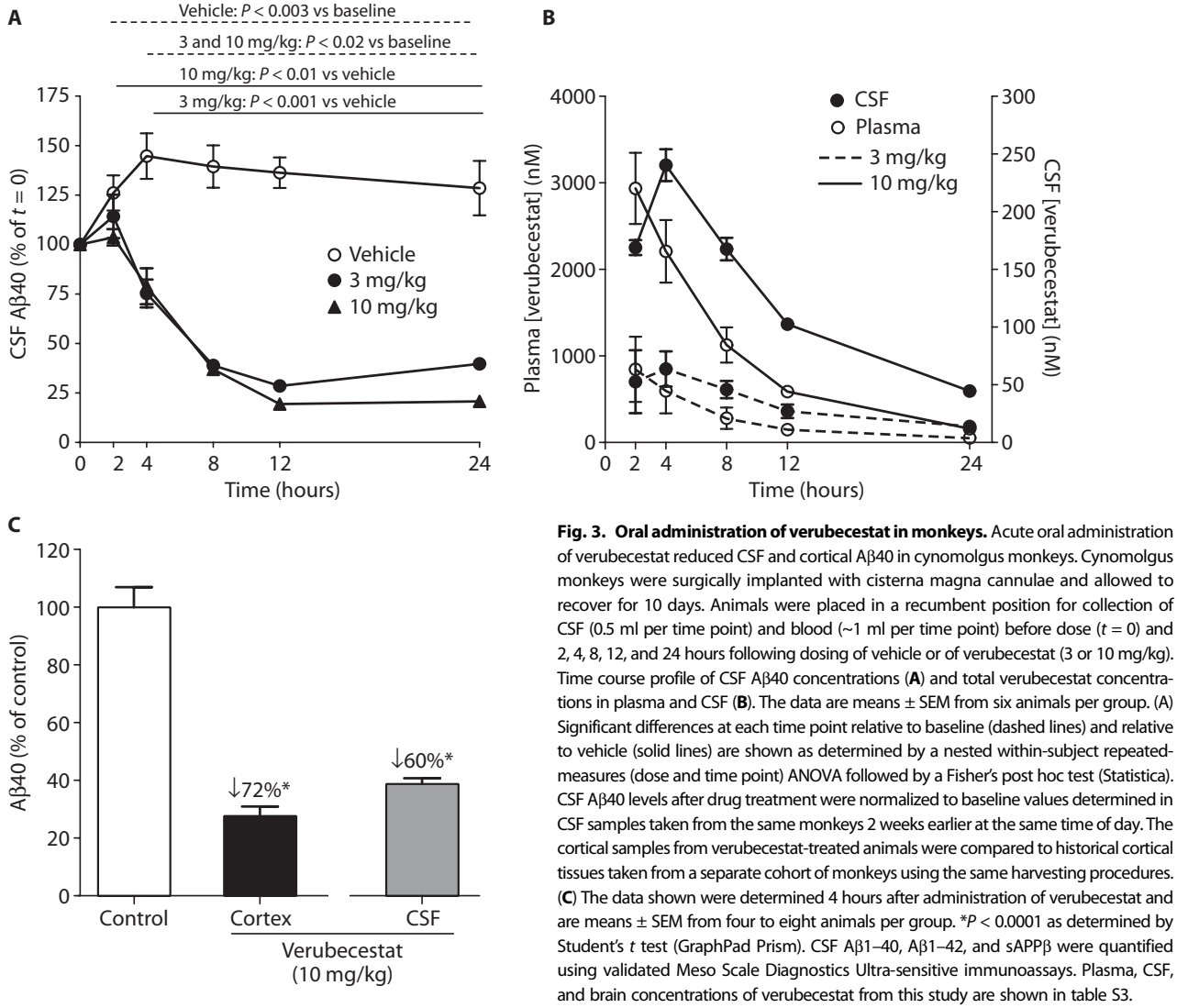

Fig. 3. Oral administration of verubecestat in monkeys. Acute oral administration of verubecestat reduced CSF and cortical Aβ40 in cynomolgus monkeys. Cynomolgus monkeys were surgically implanted with cisterna magna cannulae and allowed to recover for 10 days. Animals were placed in a recumbent position for collection of CSF (0.5 ml per time point) and blood (~1 ml per time point) before dose ($t = 0$) and 2, 4, 8, 12, and 24 hours following dosing of vehicle or of verubecestat (3 or 10 mg/kg). Time course profile of CSF Aβ40 concentrations (**A**) and total verubecestat concentrations in plasma and CSF (**B**). The data are means ± SEM from six animals per group. (A) Significant differences at each time point relative to baseline (dashed lines) and relative to vehicle (solid lines) are shown as determined by a nested within-subject repeated-measures (dose and time point) ANOVA followed by a Fisher's post hoc test (Statistica). CSF Aβ40 levels after drug treatment were normalized to baseline values determined in CSF samples taken from the same monkeys 2 weeks earlier at the same time of day. The cortical samples from verubecestat-treated animals were compared to historical cortical tissues taken from a separate cohort of monkeys using the same harvesting procedures. (**C**) The data shown were determined 4 hours after administration of verubecestat and are means ± SEM from four to eight animals per group. *$P < 0.0001$ as determined by Student's t test (GraphPad Prism). CSF Aβ1–40, Aβ1–42, and sAPPβ were quantified using validated Meso Scale Diagnostics Ultra-sensitive immunoassays. Plasma, CSF, and brain concentrations of verubecestat from this study are shown in table S3.

[1.4- to 2.1-fold based on $AUC_{(0–24\ hr)}$], consistent with the observed $t_{1/2}$. Exposures in AD patients were similar to slightly increased relative to healthy nonelderly subjects, which could either be due to the increased age of the AD patients relative to the healthy subjects or to the influence of disease. Otherwise, PK was similar between the two groups (compare tables S10 and S11).

Single and multiple doses of verubecestat were generally well-tolerated in both healthy nonelderly adults and AD patients. Adverse events were largely of mild to moderate intensity and of comparable incidence to those observed after administration of placebo (tables S12 to S14). There were no serious adverse events, discontinuations due to adverse events, or deaths. Six days after treatment with a single 550-mg dose of verubecestat, one healthy subject experienced an adverse event of macular rash and urticaria that was considered severe in intensity and possibly treatment-related. There were no clinically significant abnormalities in vital signs, laboratory parameters, or electrocardiogram parameters. However, a small increase in the Fridericia-corrected interval between the cardiac Q and T wave (QTcF interval) was observed after administration of single doses of ≥300 mg, with the mean increase in QTcF interval ranging from 6.5 to 15.5 ms. By contrast, QTc prolongation was not observed after administration of multiple doses of up to 250 mg for 14 days.

PK/PD modeling to select doses and infer brain effects of verubecestat

A prospectively planned mechanistic PK/PD modeling effort using data across all time points, CSF PD end points, and three phase 1 studies was conducted to develop an integrated characterization of verubecestat effects in humans (see fig. S8 for a model schematic). The model was used to interpret verubecestat effects on CSF Aβ40, Aβ42, and sAPPβ in the context of modulation of the de novo brain production of these APP metabolites and to aid in the selection of verubecestat doses for later-stage clinical trials.

The model accurately represents the time course of verubecestat effects on CSF concentrations of all three APP metabolites via a single drug action, namely BACE1 inhibition in the brain (fig. S9). Similar potency estimates (IC_{50}) were obtained in AD patients relative to healthy subjects (table S15). In contrast, the maximal reduction (E_{max}) values, which are expected to reflect the fraction of baseline concentrations of CSF Aβ40, Aβ42, and sAPPβ resulting from de novo brain production,

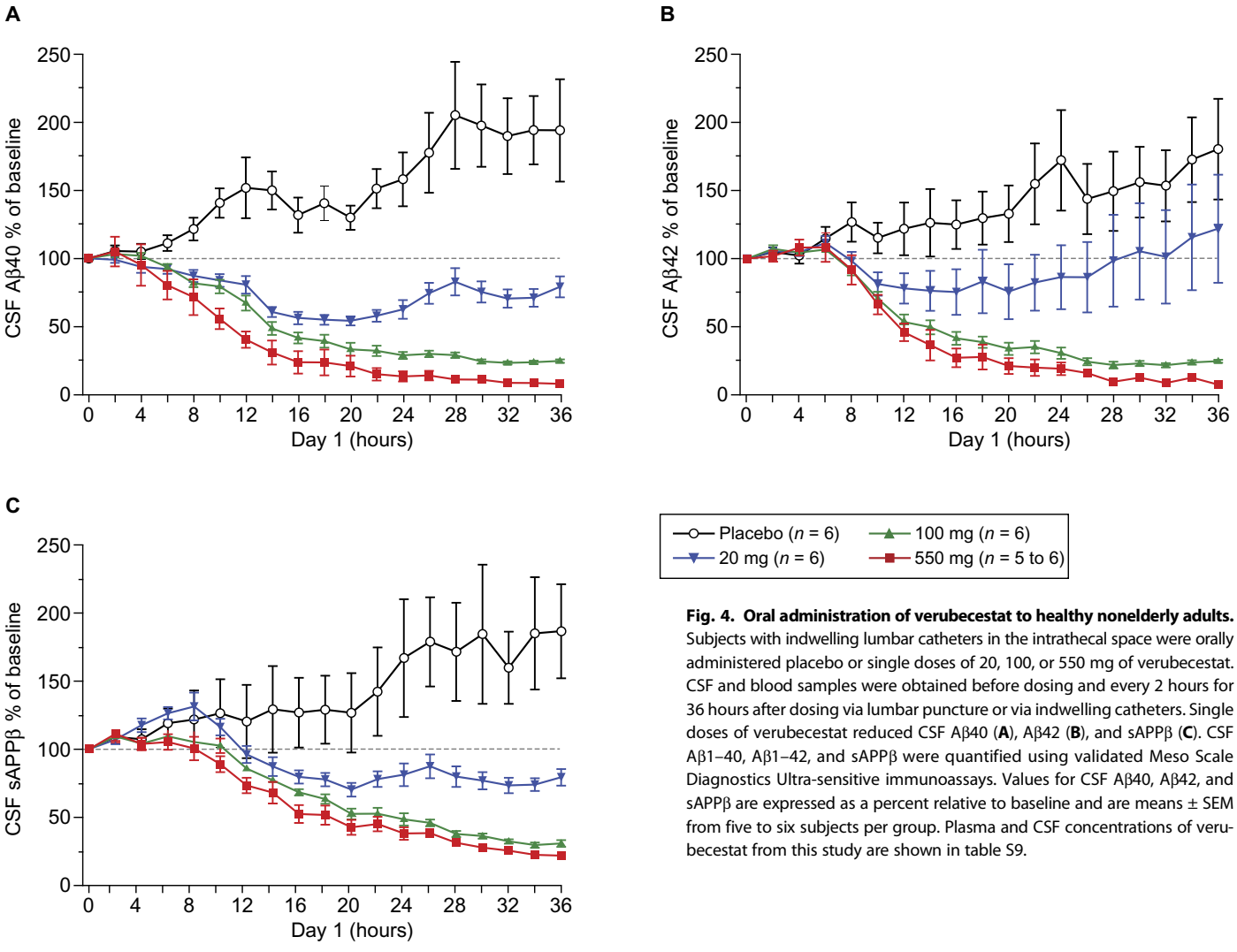

Fig. 4. Oral administration of verubecestat to healthy nonelderly adults. Subjects with indwelling lumbar catheters in the intrathecal space were orally administered placebo or single doses of 20, 100, or 550 mg of verubecestat. CSF and blood samples were obtained before dosing and every 2 hours for 36 hours after dosing via lumbar puncture or via indwelling catheters. Single doses of verubecestat reduced CSF Aβ40 (**A**), Aβ42 (**B**), and sAPPβ (**C**). CSF Aβ1–40, Aβ1–42, and sAPPβ were quantified using validated Meso Scale Diagnostics Ultra-sensitive immunoassays. Values for CSF Aβ40, Aβ42, and sAPPβ are expressed as a percent relative to baseline and are means ± SEM from five to six subjects per group. Plasma and CSF concentrations of verubecestat from this study are shown in table S9.

tended to be lower in AD patients relative to healthy subjects. This was especially true for Aβ42, where this variation between healthy subjects and AD patients (0.91 versus 0.96) was associated with nonoverlapping 95% confidence intervals, which is suggestive of a real difference.

Because the model included integrated variability terms that were informed by all subjects enrolled across the three phase 1 studies, model-based simulations are informative of the likely response distribution despite the small size of each dose group in the phase 1 studies. Consistent with the observed reduction of CSF Aβ40 in AD patients (Fig. 6), model-based prediction of the verubecestat dose-response relationship (Fig. 7A) and distribution of individual responses (Fig. 7B) indicated that 12 mg daily would produce partial reduction in CSF Aβ40 (96.6% of AD patients with CSF Aβ40 reduction of 50 to 75%; average reduction, 67.1%), whereas 40 mg daily would produce near-maximal CSF Aβ40 reduction that is meaningfully different from 12 mg (94.6% of AD patients with CSF Aβ40 reduction of 80 to 90%; average reduction, 83.7%). The model predicts a slightly greater reduction of de novo brain Aβ40 production relative to CSF Aβ40 reduction at these two doses (average reductions of 72.2 and 90.1% at the 12- and 40-mg doses, respectively; Fig. 7B).

DISCUSSION

Despite the large body of evidence supporting the amyloid hypothesis of AD pathogenesis, efforts to develop agents that safely and unambiguously reduce CNS concentrations of Aβ in humans have not been successful to date. Although this lack of success has been cited as evidence against the amyloid hypothesis, the treatments evaluated to date have lacked convincing evidence of substantial and sustained CNS Aβ reduction at doses having an acceptable tolerability profile (*2*, *24*). Given the required role of BACE1 in Aβ production, inhibition of this enzyme has long been viewed as a promising Aβ-lowering therapeutic target, but several obstacles have prevented BACE1 inhibitors from advancing to pivotal clinical trials (*3*, *12*). Our efforts to develop potent, selective, orally bioavailable BACE1 inhibitors that safely reduce Aβ in the CNS culminated in the discovery of verubecestat (*13*). Verubecestat inhibits BACE1 with similar potency in a purified enzyme assay and in intact cells. This suggests that the compound can traverse the multiple membranes required to access BACE1 in cells, consistent with its high permeability. Verubecestat also proved to be a potent and effective inhibitor of plasma, CSF, and cortical Aβ40, Aβ42, and sAPPβ production in both rats and monkeys, achieving >90% reduction in all three compartments. Its ability

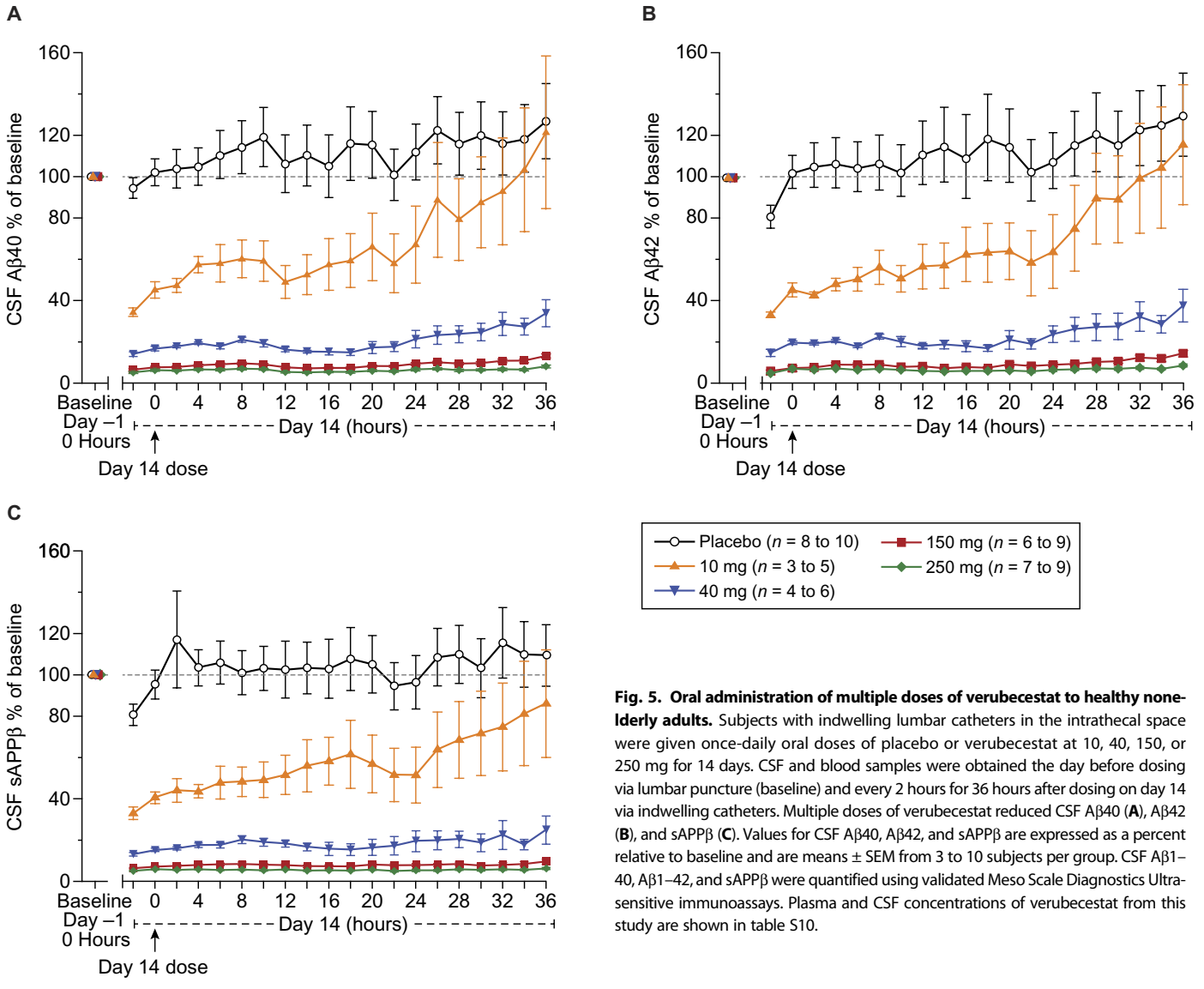

Fig. 5. Oral administration of multiple doses of verubecestat to healthy nonelderly adults. Subjects with indwelling lumbar catheters in the intrathecal space were given once-daily oral doses of placebo or verubecestat at 10, 40, 150, or 250 mg for 14 days. CSF and blood samples were obtained the day before dosing via lumbar puncture (baseline) and every 2 hours for 36 hours after dosing on day 14 via indwelling catheters. Multiple doses of verubecestat reduced CSF Aβ40 (**A**), Aβ42 (**B**), and sAPPβ (**C**). Values for CSF Aβ40, Aβ42, and sAPPβ are expressed as a percent relative to baseline and are means ± SEM from 3 to 10 subjects per group. CSF Aβ1–40, Aβ1–42, and sAPPβ were quantified using validated Meso Scale Diagnostics Ultrasensitive immunoassays. Plasma and CSF concentrations of verubecestat from this study are shown in table S10.

to reduce CSF and brain concentrations of Aβ40, Aβ42, and sAPPβ in animals was maintained after chronic treatment, indicating that no compensatory biological processes overcome the effects of BACE1 inhibition. Verubecestat was substantially more potent in reducing plasma Aβ40 than in reducing CSF or brain Aβ40, at least in part, because verubecestat is a substrate of P-glycoprotein, which transports compounds out of the brain (see below).

Administration of both single and multiple doses of verubecestat to healthy adult volunteers reduced plasma and CSF levels of Aβ40, Aβ42, and sAPPβ in a dose-dependent manner, with the highest doses achieving ≥90% reduction. The potency and maximal effect of verubecestat to reduce plasma and CSF concentrations of Aβ40, Aβ42, and sAPPβ were similar in humans and animals, and the observed human $t_{1/2}$, dose, and plasma C_{max} and AUC required to achieve the targeted reduction of CSF Aβ40 were also similar to the predictions derived from animal studies. This concordance highlights the value of measuring identical end points in animal and human studies, a practice that should greatly improve the historically poor clinical translation in neuroscience drug development programs. As in the in vitro and animal studies, the potencies and maximal effects of verubecestat in reducing CSF Aβ40, Aβ42, and sAPPβ in humans were comparable, and the degrees of reduction were highly correlated. Furthermore, the PK/PD modeling suggested that verubecestat effects on all three APP metabolites could be interpreted via a single drug action, that is, BACE1 inhibition in the brain. Therefore, these data suggest that measurement of any one of these three APP metabolites is a suitable surrogate for assessment of BACE1 inhibition in humans. The ability of the model to interpret the data based on BACE1 inhibition alone suggests that a substrate (APP) does not accumulate in humans after BACE1 inhibition, probably because of compensatory metabolism by other pathways [for example, the α-secretase pathway or the more recently described η-secretase pathway (*25*, *26*)]. This is in contrast to γ-secretase inhibition where the potentially neurotoxic substrate C99 accumulates substantially [for example, (*27*)]. Although verubecestat is a P-glycoprotein substrate, its potency and maximal effect in lowering CSF and brain Aβ and sAPPβ were very similar in animals and were achieved at submicromolar total plasma concentrations. Furthermore, PK/PD modeling

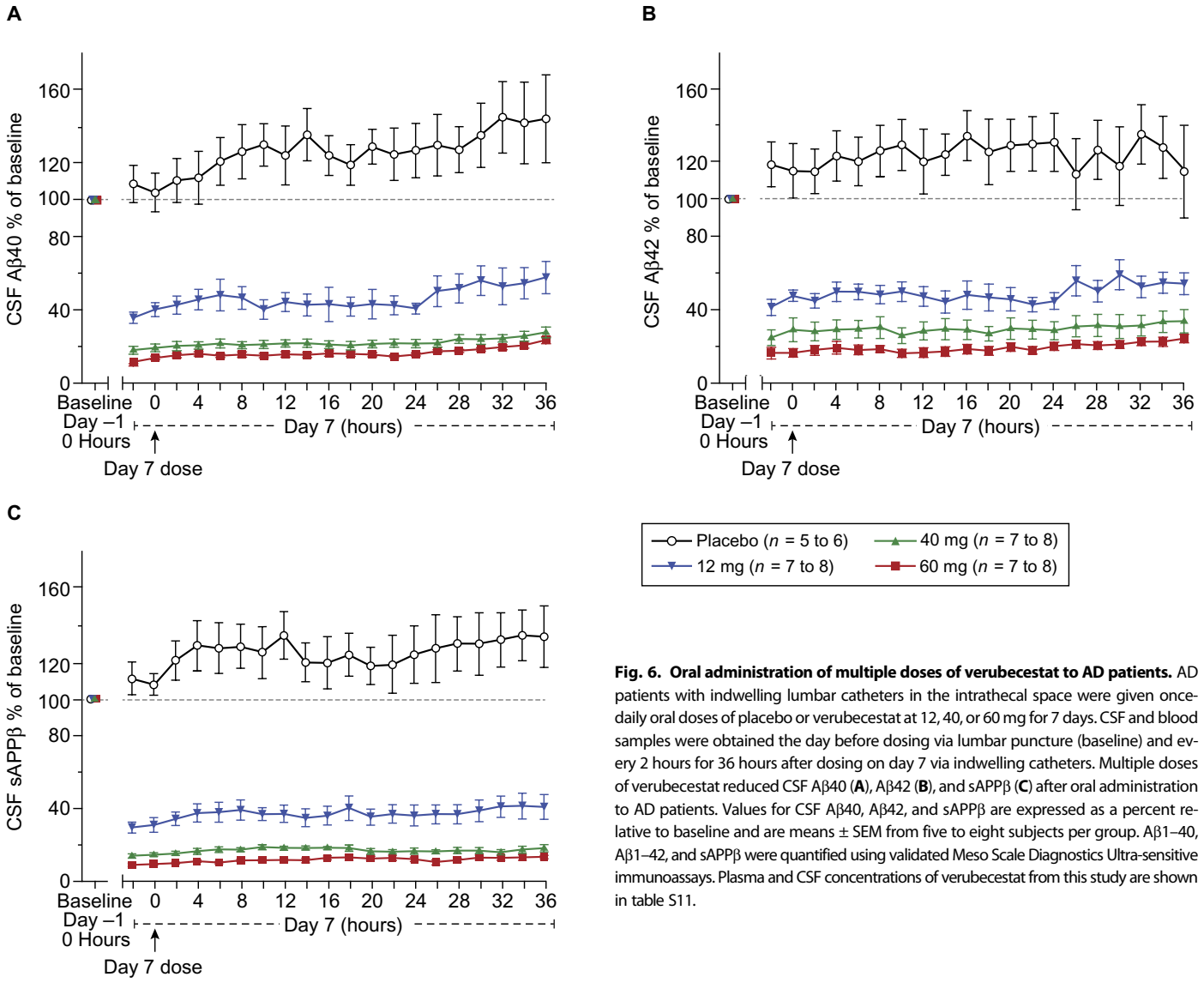

Fig. 6. Oral administration of multiple doses of verubecestat to AD patients. AD patients with indwelling lumbar catheters in the intrathecal space were given once-daily oral doses of placebo or verubecestat at 12, 40, or 60 mg for 7 days. CSF and blood samples were obtained the day before dosing via lumbar puncture (baseline) and every 2 hours for 36 hours after dosing on day 7 via indwelling catheters. Multiple doses of verubecestat reduced CSF Aβ40 (**A**), Aβ42 (**B**), and sAPPβ (**C**) after oral administration to AD patients. Values for CSF Aβ40, Aβ42, and sAPPβ are expressed as a percent relative to baseline and are means ± SEM from five to eight subjects per group. Aβ1–40, Aβ1–42, and sAPPβ were quantified using validated Meso Scale Diagnostics Ultra-sensitive immunoassays. Plasma and CSF concentrations of verubecestat from this study are shown in table S11.

of the human data suggests that verubecestat has comparable ability to reduce de novo brain production and CSF levels of Aβ40, Aβ42, and sAPPβ. These data suggest that high BACE1 affinity and high permeability of verubecestat can overcome CNS efflux mediated by P-glycoprotein and that measurement of CSF Aβ40, Aβ42, and sAPPβ is a reasonable surrogate for verubecestat effects on brain concentrations of these APP metabolites in humans. At doses of ≥20 to 40 mg, reduction of CSF Aβ and sAPPβ was sustained for at least 24 hours and unbound trough (C_{24hr}) plasma, and CSF concentrations of verubecestat were at or above the in vitro IC_{50}. Along with the observed human $t_{1/2}$ (14 to 24 hours), these data confirm that verubecestat can be dosed once per day.

This report also describes testing of BACE inhibition in AD patients, which was considered critical for a number of reasons. Unlike healthy adults, AD patients have a large reservoir of oligomeric, fibrillar, and plaque-borne Aβ in the brain, which may contribute to CSF levels and may be refractory to short-term inhibition of BACE1. BACE1 protein and enzymatic activity are also up-regulated in the brains of AD patients, particularly around amyloid plaques (*28*). Finally, AD patients may be more susceptible to drug-induced adverse effects than healthy subjects. Overall, the safety and effect of verubecestat on Aβ40, Aβ42, and sAPPβ in CSF were very similar in AD patients and healthy adults. The estimated potency (IC_{50}) of verubecestat was comparable in healthy adults and AD patients, suggesting that the disease has no impact on the ability of verubecestat to inhibit BACE1. The E_{max} value of CSF Aβ42 was slightly less in AD subjects than in healthy adults. Because E_{max} values represent the contribution of de novo Aβ42 production, this suggests a small (~10%) contribution of dissociation of oligomeric, plaque-derived, or other slowly cleared sources of Aβ42 to the CSF Aβ42 pool in AD patients. Experimental and modeling studies suggest that these slowly cleared sources of Aβ42 may be reduced over time by chronic BACE inhibition (*22*, *25*).

Many previously studied anti-amyloid mechanisms, most notably γ-secretase inhibitors and anti-Aβ antibodies, are associated with serious side effects that limit the dose that can be administered to humans (*5*, *24*). Several recent publications have described adverse phenotypes of Bace1

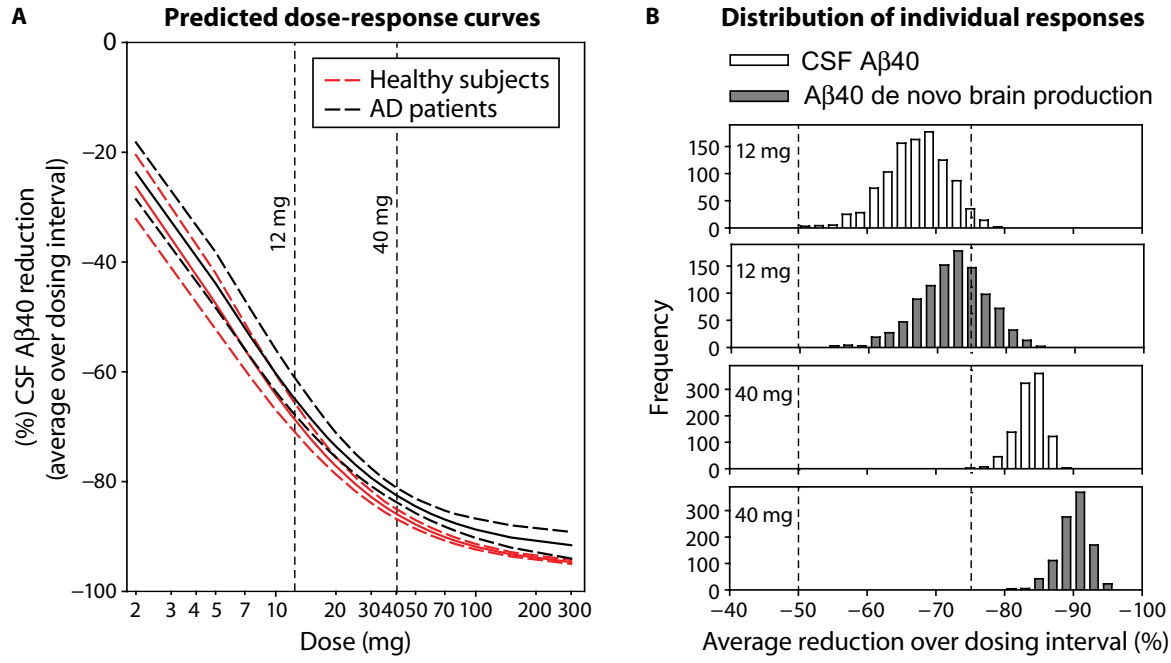

Fig. 7. Simulated steady-state verubecestat dose-response curves and predicted distribution of individual responses. A prospectively planned mechanistic PK/PD model was generated that used data across all time points, CSF PD end points, and studies to develop an integrated characterization of verubecestat effects in humans. (**A**) The solid and dashed lines represent the median and 90% confidence interval, respectively, of 1000 replicates of the response in a typical AD patient (black line) and a healthy nonelderly adult subject (red line). (**B**) Simulated distributions of individual CSF Aβ40 and de novo brain Aβ40 production in AD patients (n = 1000 subjects per dose level).

and Bace2 knockout mice, as well as new BACE1/BACE2 substrates and new Aβ fragments whose modulation by BACE inhibition has the potential to induce side effects [(*29*, *30*); for reviews, see (*3*, *12*)]. In addition, several BACE inhibitors have caused adverse effects in animal or human studies, although, in at least some cases, these effects appear unrelated to BACE inhibition (*12*, *14*, *31*). Thus, the relatively benign preclinical and clinical safety profile of verubecestat is noteworthy. In particular, reduced central and peripheral nerve myelination (*17*, *18*), retinal degeneration (*32*), reduced blood glucose and increased pancreatic β cell mass (*19*), and brain neurodegeneration (*14*, *33*) have been reported after genetic deletion or pharmacological inhibition of BACE1 and/or BACE2, but none of these effects were observed after chronic treatment of rats and monkeys with verubecestat. Clinical development of the BACE inhibitor LY2886721 was terminated because of hepatotoxicity (*31*), but there was no evidence of hepatotoxicity in the animal or human studies of verubecestat reported here, although longer-term treatment is required to definitively assess hepatotoxicity in humans. As previously reported for another BACE inhibitor (*20*), chronic verubecestat administration resulted in fur (but not skin or eye) hypopigmentation in rodents and rabbits. The variegated pattern of hypopigmentation is likely due to the random nature of the hair follicle cycle, which controls both hair replacement and pigmentation (*20*). The role of BACE2 in rodent fur pigmentation is now well-documented (*20*, *21*), and the higher affinity of verubecestat for BACE2 relative to BACE1 likely contributes to the hypopigmentation observed after verubecestat treatment. However, inhibition of BACE1 by verubecestat also likely contributes to hypopigmentation as recently documented (*20*) and consistent with our in-house results. The relevance of fur hypopigmentation to humans is unclear because fur or skin pigmentation changes were not observed in monkeys treated with verubecestat for 9 months, and there were no reports of changes in skin or hair pigmentation in the human studies with verubecestat described here. However, treatment of humans for more than the 14 days reported here is likely required to observe pigmentation changes; therefore, skin and hair pigmentation status have been routinely monitored in the ongoing clinical trials of verubecestat. Further details of studies examining the role of BACE1 and BACE2 in hypopigmentation, phenotypes of Bace1 and Bace2 knockout mice, and chronic treatment of animals with BACE inhibitors will be the subject of forthcoming publications.

There are several possible reasons for the discrepancy between the benign safety profile of verubecestat and the expected safety issues suggested by Bace1/Bace2 knockout mice, non-APP BACE1/BACE2 substrates, new Aβ fragments, and experience with other BACE inhibitors. First, verubecestat is very selective for BACE1 over a host of off-target proteins. The >45,000-fold selectivity of verubecestat for BACE1 over CatD is especially important given the toxicities observed after genetic deletion of CatD and after pharmacological inhibition of CatD in animals treated with the less selective or lysosomotropic BACE inhibitors LY2811376, AMG-8718, and PF-9283 (*14*, *34*–*36*, and references therein). The exquisite BACE enzyme selectivity of verubecestat is likely driven by differences in the $S3^{sp}$ subsite between BACE1 and CatD (see Fig. 1D) (*13*). Second, phenotypes of knockout mice often depend on the genetic background of the mice and may reflect developmental effects that are not recapitulated upon knockout or pharmacological inhibition of the target in adult animals (*37*). BACE1 is expressed at markedly higher levels in early pre- and postnatal development relative to adult animals (*17*). Knockout mice also have complete loss of BACE1 and/or BACE2 activity, which cannot practically be achieved via pharmacological inhibition and which may not be necessary for therapeutic effect. Third, the physiological relevance of new APP fragments and BACE1/ BACE2 substrates whose processing may be modulated by verubecestat is not yet well understood. Many of the BACE1 and BACE2 substrates that have been

reported are processed by other proteases, which may compensate for lack of BACE1 or BACE2 activity [for example, (*38*)]. Despite the plethora of reported γ-secretase substrates, most, if not all, of the side effects of γ-secretase inhibitors can be definitively or plausibly linked to inhibition of Notch processing (*39*), suggesting caution in making premature conclusions about adverse events arising from inhibition of the processing of reported BACE1 and BACE2 substrates. On the other hand, it should also be noted that inhibition of the processing of some of the reported substrates of BACE1 and BACE2 may result in subtle phenotypes that do not overtly alter animal behavior and that require very specific and detailed histopathological analysis [for example, axon guidance defects due to inhibition of CHL1 processing (*29*)]. The availability of high-quality BACE inhibitors like verubecestat will facilitate future work aimed at better understanding the physiological role of new BACE1/2 substrates and clarifying any potential adverse events that may result from BACE inhibition.

Apart from inhibition of BACE2, the only significant off-target activity of verubecestat is inhibition of the hERG channel, which is a common cause of QTc prolongation and associated cardiac arrhythmias. However, the in vitro IC_{50} of verubecestat at the hERG channel (2.2 μM) is well above the total and unbound C_{max} (248 and 87 nM, respectively) observed at the highest dose (40 mg) being tested in the ongoing phase 3 trials [see also (*13*)]. QTc prolongation was only observed in humans in this study at doses or exposures much higher than those being tested in the ongoing verubecestat clinical trials.

Because of its favorable initial safety profile and its ability to markedly reduce CSF Aβ and sAPPβ concentrations, verubecestat was the first BACE inhibitor to progress to phase 3 clinical trials. The EPOCH phase 2/3 trial (ClinicalTrials.gov identifier: NCT01739348) is testing the impact of 18 months of treatment with 12 and 40 mg of verubecestat on cognitive and functional measures in ~2000 subjects with mild to moderate AD. Because the degree of Aβ reduction required to improve cognition and/or slow the progression of AD is unknown and because there may be unforeseen adverse effects of chronic, nearly complete BACE1 inhibition in humans, the 12- and 40-mg doses will test the effects of both partial and near-maximal Aβ reduction. Partial reduction of Aβ has positive effects on cognition and plaque levels in animal models (*7*, *8*), and human genetic data suggest that modest changes in Aβ production significantly modify the risk of AD (*5*, *9*). The first stage of the EPOCH trial included a safety cohort of 200 patients treated for 3 months, some of whom were treated with a higher dose of 60 mg. The 60-mg dose was tested to further explore the safety of verubecestat, including safety in patients administered 12- and 40-mg doses who will attain higher-than-average exposures. When considered along with the safety profile of verubecestat in animals and in human phase 1 studies, the results supported proceeding to enrollment of the full trial. Because deposition of amyloid begins several years before AD is diagnosed, it is possible that administration of an anti-amyloid agent will be more effective if given early in the disease process (*5*). Consequently, the APECS phase 3 trial (ClinicalTrials.gov identifier: NCT01953601) is being conducted to test the effect of 2 years of treatment with 12 and 40 mg of verubecestat on cognitive and functional measures in ~1500 subjects with prodromal AD who have significant amyloid deposition, as measured by amyloid positron emission tomography imaging. Given that the doses being tested in the ongoing phase 3 trials reduce CSF Aβ by >80% and assuming that the compound continues to demonstrate an acceptable safety and tolerability profile, these trials will be able to determine whether verubecestat can be a much-needed disease-modifying treatment for AD. These trials should also be able to test the validity of the amyloid hypothesis in various populations of AD patients (that is, asymptomatic, prodromal, and mild/moderate AD patients).

MATERIALS AND METHODS

Study design

The studies described in this manuscript were conducted to characterize the safety, tolerability, and PD effects of verubecestat in animals, healthy human subjects, and AD patients. The sample size for animal experiments was based on previous experience and used the minimum number of animals required to obtain a significant difference based on the expected effect size and variability. All animal and human studies were conducted once; additional animal studies that used some of the reported verubecestat doses and time points were consistent with the reported results. It was not considered necessary to replicate each animal and human study with verubecestat because of experience with other BACE inhibitors in similar studies and because of a desire to minimize animal use and human exposure. Aβ40, Aβ42, and sAPPβ measurements from each subject and time point were measured in duplicate, whereas a single PK measurement from each subject and time point was done. Data were only excluded in the case of CSF samples that had blood contamination upon visual inspection. No outliers were excluded. The personnel were blind to treatment in all animal studies but were not blinded in the case of Aβ40, Aβ42, sAPPβ, and PK measurements. Further details of the animal studies are described below. All human clinical studies were randomized, double-blind, and placebo-controlled and were conducted in accordance with principles of Good Clinical Practice. The human studies were approved by the appropriate institutional review committees and regulatory agencies, and written informed consent was obtained from each subject or their legal representative (in the case of AD patients) before any study procedures. For further details, see the Supplementary Materials and Methods and the accompanying clinical protocols.

Materials

Verubecestat was synthesized as described (*13*). Purified human BACE1 and BACE2 soluble N-terminal catalytic domains, human CatD, human CatE, human pepsin, and human renin were prepared or sourced as previously described (*40*, *41*).

In vitro assays

Inhibitor K_i values at human BACE1 and other human aspartyl proteases were determined as previously described (*40*, *41*). The inhibitor IC_{50} values for reduction of Aβ40, Aβ42, and sAPPβ production in HEK293-$APP^{swe/lon}$ cells were determined as previously described (*42*).

Animal care and use

All rat studies were approved by the Merck Institutional Animal Care and Use Committee (IACUC) and were conducted in an American Association for Accreditation of Laboratory Animal Care–accredited facility in accordance with the National Institutes of Health *Guide to the Care and Use of Laboratory Animals* and the Animal Welfare Act. The cynomolgus monkey CSF time course study was conducted at Maccine Pte. Ltd. (Singapore) and was approved by their internal IACUC.

In vivo effects of verubecestat

Verubecestat-HCl was dissolved or suspended in either 20% hydroxypropyl-β-cyclodextrin or 0.5% methylcellulose. Control animals were treated with the appropriate vehicle.

In vivo rodent and cynomolgus monkey PK and PD studies were carried out essentially as described previously (*13*, *40*, *42*). In vivo animal toxicity studies were performed in Sprague-Dawley rats for 6 months (0, 5, 25, or 75 mg kg^{-1} day^{-1}; 15 animals per sex per group) and in cynomolgus monkeys for 9 months (0, 10, 30, or 100 mg kg^{-1} day^{-1}; 4 animals per sex per group). An exploratory study was conducted in pigmented Dutch belted rabbits (0 or 75 mg kg^{-1} day^{-1} for 4 months; 24 female animals per group) to assess hypopigmentation of the black hair coat, which was originally observed in an embryo-fetal developmental toxicity study.

Quantitation of Aβ40, Aβ42, and sAPPβ

Aβ40 in rat and Aβ40, Aβ42, and sAPPβ in cynomolgus monkey were measured as described previously (*40*, *42*). Rat and monkey samples were assayed at Merck, whereas human samples were assayed at Tandem Laboratories (San Diego, CA, USA) using commercially available Meso Scale Diagnostics Ultra-sensitive immunoassays that were batch-tested following protocols that were validated at Merck Research Laboratories.

Mechanistic PK/PD model of verubecestat clinical data

The exposure-response relationship for CSF Aβ40, Aβ42, and sAPPβ modulation by verubecestat was evaluated using a population modeling approach (NONMEM version 7.1). A mechanistic model was developed that simultaneously described CSF Aβ40, sAPPβ, and Aβ42 response as a function of verubecestat plasma exposure (fig. S7). Modulation of brain Aβ40, Aβ42, and sAPPβ was related to plasma verubecestat concentrations by separate sigmoid E_{max} functions and a joint IC_{50} parameter, which accounted for the in vivo potency and efficacy of verubecestat action on all three biomarkers with good precision (table S15). The observed lag time between maximal plasma concentration and maximal effects on the CSF biomarkers was accounted for by a transit model representing the delay between inhibition of BACE1 in the brain and lumbar CSF biomarker responses. Baseline drift—generally apparent as monotonic increasing CSF Aβ40, sAPPβ, and Aβ42 levels over time in patients on placebo (*14*, *23*)—was included as an additive empirical time-dependent model. Model qualification was performed with model diagnostic plots to illustrate goodness of fit, whereas accuracy and robustness of the model was assessed by visual predictive checks and a nonparametric bootstrap analysis.

The established PK/PD model was used to predict the median dose-response profile for verubecestat reduction of CSF sAPPβ, Aβ40, and Aβ42 at steady state in the typical healthy subject and AD patient. Reduction of CSF sAPPβ, Aβ40, and Aβ42 was simulated for 1000 replicates at each dose level of verubecestat. For each replicate, a PD parameter vector was sampled from the bootstrap results from the final PK/PD model to account for estimation uncertainty. The CSF sAPPβ, Aβ40, and Aβ42 profiles at steady state were then simulated, and the TWA level of reduction during the dosing interval was calculated relative to placebo.

Model-based simulations were conducted to predict the distribution of individual Aβ40 responses in the AD patient population. Verubecestat exposure at steady state was simulated at daily doses of 12 and 40 mg (n = 1000 subjects per dose level). These simulations incorporated interindividual variability in PK parameters and effects of demographic factors. Virtual AD patients were generated by sampling with replacement from the demographic data for gender, age, and weight from two previous Merck trials in AD patients and from the multiple-dose verubecestat study in AD patients described herein. The PK/PD model was used to predict individual CSF Aβ40 responses and de novo brain Aβ40 production responses (expressed as TWA relative to placebo) based on the individual predicted verubecestat exposures.

Statistical analysis

Dunnett's multiple comparison test (GraphPad Prism) was applied to the rat time course study with $\alpha = 0.05$. Student's t test (GraphPad Prism) was applied to all between-group measures with $\alpha = 0.05$. For the single oral dose time course study of verubecestat in cynomolgus monkeys, an analysis of between-group differences at each time point relative to baseline and relative to vehicle treatment was determined by a nested within-subject repeated-measures (dose and time point) ANOVA followed by a Fisher's post hoc test (Statistica). Details of the statistical analyses applied to each data set, the number of subjects, and the resulting P values are described in the figure legends. All data plotted for clinical studies are means ± SEM for each group.

SUPPLEMENTARY MATERIALS

www.sciencetranslationalmedicine.org/cgi/content/full/8/363/363ra150/DC1

Materials and Methods

Fig. S1. Time course of total plasma (closed circles), brain (open circles), and CSF (stars) concentrations of verubecestat after oral administration of a single dose to rats.

Fig. S2. Effect of oral administration of a single dose of verubecestat on CSF sAPPβ concentrations in cisterna magna–cannulated cynomolgus monkeys.

Fig. S3. Chronic (9-month) oral administration of verubecestat reduces CSF and cortical Aβ40, Aβ42, and sAPPβ in cynomolgus monkeys.

Fig. S4. Chronic (3-month) oral administration of verubecestat reduces cortical Aβ40 in rats.

Fig. S5. Chronic verubecestat treatment causes fur hypopigmentation in Dutch belted rabbits.

Fig. S6. Single doses of verubecestat reduce plasma Aβ40 after oral administration to healthy nonelderly adults.

Fig. S7. Multiple doses of verubecestat reduce plasma Aβ40 after oral administration to healthy nonelderly adults.

Fig. S8. Schematic of the amyloid dynamics model.

Fig. S9. Model-based representation of verubecestat effects on CSF Aβ40, Aβ42, and sAPPβ in the three phase 1 studies.

Table S1. Activity of verubecestat at additional targets.

Table S2. Total plasma, CSF, and brain concentrations of verubecestat after acute oral administration to rats.

Table S3. Total plasma, CSF, and brain concentrations of verubecestat after acute oral administration to cynomolgus monkeys.

Table S4. Total plasma, CSF, and brain concentrations of verubecestat after chronic oral administration to cynomolgus monkeys.

Table S5. Total plasma and brain concentrations of verubecestat after chronic oral administration to rats.

Table S6. Animal PK properties of verubecestat.

Table S7. Serum glucose concentrations after chronic treatment of rats with verubecestat for 6 months.

Table S8. Serum glucose concentrations after chronic treatment of monkeys with verubecestat for 9 months.

Table S9. PK of verubecestat after single-dose administration to healthy nonelderly adults (experiment shown in Fig. 4).

Table S10. PK of verubecestat after multiple-dose administration to healthy nonelderly adults (day 14) (experiment shown in Fig. 5).

Table S11. PK of verubecestat after multiple-dose administration to patients with AD (day 7) (experiment shown in Fig. 6).

Table S12. Number (%) of healthy nonelderly adults with adverse events after administration of single oral doses of verubecestat.

Table S13. Number (%) of healthy nonelderly adults with adverse events in the multiple-dose study after once-daily oral administration of verubecestat for 14 days.

Table S14. Number (%) of AD patients with adverse events after once-daily oral administration of verubecestat for 7 days.

Table S15. Model-based estimates of verubecestat effects on de novo brain production of Aβ40, Aβ42, and sAPPβ in humans.

REFERENCES AND NOTES

1. H. Braak, D. R. Thal, E. Ghebremedhin, K. Del Tredici, Stages of the pathologic process in Alzheimer disease: Age categories from 1 to 100 years. *J. Neuropathol. Exp. Neurol.* **70**, 960–969 (2011).

2. D. J. Selkoe, J. Hardy, The amyloid hypothesis of Alzheimer's disease at 25 years. *EMBO Mol. Med.* **8**, 595–608 (2016).
3. R. Yan, R. Vassar, Targeting the β secretase BACE1 for Alzheimer's disease therapy. *Lancet Neurol.* **13**, 319–329 (2014).
4. D. J. Selkoe, Soluble oligomers of the amyloid β-protein impair synaptic plasticity and behavior. *Behav. Brain Res.* **192**, 106–113 (2008).
5. E. S. Musiek, D. M. Holtzman, Three dimensions of the amyloid hypothesis: Time, space and 'wingmen'. *Nat. Neurosci.* **18**, 800–806 (2015).
6. D. Dominguez, J. Tournoy, D. Hartmann, T. Huth, K. Cryns, S. Deforce, L. Serneels, I. E. Camacho, E. Marjaux, K. Craessaerts, A. J. Roebroek, M. Schwake, R. D'Hooge, P. Bach, U. Kalinke, D. Moechars, C. Alzheimer, K. Reiss, P. Saftig, B. De Strooper, Phenotypic and biochemical analyses of BACE1- and BACE2-deficient mice. *J. Biol. Chem.* **280**, 30797–30806 (2005).
7. M. Ohno, S. L. Cole, M. Yasvoina, J. Zhao, M. Citron, R. Berry, J. F. Disterhoft, R. Vassar, BACE1 gene deletion prevents neuron loss and memory deficits in 5XFAD APP/PS1 transgenic mice. *Neurobiol. Dis.* **26**, 134–145 (2007).
8. L. McConlogue, M. Buttini, J. P. Anderson, E. F. Brigham, K. S. Chen, S. B. Freedman, D. Games, K. Johnson-Wood, M. Lee, M. Zeller, W. Liu, R. Motter, S. Sinha, Partial reduction of BACE1 has dramatic effects on Alzheimer plaque and synaptic pathology in APP transgenic mice. *J. Biol. Chem.* **282**, 26326–26334 (2007).
9. T. Jonsson, J. K. Atwal, S. Steinberg, J. Snaedal, P. V. Jonsson, S. Bjornsson, H. Stefansson, P. Sulem, D. Gudbjartsson, J. Maloney, K. Hoyte, A. Gustafson, Y. Liu, Y. Lu, T. Bhangale, R. R. Graham, J. Huttenlocher, G. Bjornsdottir, O. A. Andreassen, E. G. Jönsson, A. Palotie, T. W. Behrens, O. T. Magnusson, A. Kong, U. Thorsteinsdottir, R. J. Watts, K. Stefansson, A mutation in *APP* protects against Alzheimer's disease and age-related cognitive decline. *Nature* **488**, 96–99 (2012).
10. I. Benilova, R. Gallardo, A.-A. Ungureanu, V. Castillo Cano, A. Snellinx, M. Ramakers, C. Bartic, F. Rousseau, J. Schymkowitz, B. De Strooper, The Alzheimer disease protective mutation A2T modulates kinetic and thermodynamic properties of amyloid-β (Aβ) aggregation. *J. Biol. Chem.* **289**, 30977–30989 (2014).
11. J. A. Maloney, T. Bainbridge, A. Gustafson, S. Zhang, R. Kyauk, P. Steiner, M. van der Brug, Y. Liu, J. A. Ernst, R. J. Watts, J. K. Atwal, Molecular mechanisms of Alzheimer disease protection by the A673T allele of amyloid precursor protein. *J. Biol. Chem.* **289**, 30990–31000 (2014).
12. S. Barão, D. Moechars, S. F. Lichtenthaler, B. De Strooper, BACE1 physiological functions may limit its use as therapeutic target for Alzheimer's disease. *Trends Neurosci.* **39**, 158–169 (2016).
13. J. D. Scott, S. W. Li, A. P. J. Brunskill, X. Chen, K. Cox, J. N. Cumming, M. Forman, E. J. Gilbert, R. Hodgson, L. A. Hyde, Q. Jiang, U. Iserloh, I. Kazakevich, R. Kuvelkar, H. Mei, J. Meredith, J. Misiaszek, P. Orth, L. M. Rossiter, M. Slater, J. Stone, C. Strickland, J. H. Voigt, G. Wang, H. Wang, Y. Wu, W. J. Greenlee, E. M. Parker, M. E. Kennedy, A. W. Stamford, Discovery of the 3-imino-1,2,4-thiadiazinane 1,1-dioxide derivative verubecestat (MK-8931)—A β-site amyloid precursor protein cleaving enzyme 1 inhibitor for the treatment of Alzheimer's disease. *J. Med. Chem.*, 10.1021/acs.jmedchem.6b00307 in press.
14. P. C. May, R. A. Dean, S. L. Lowe, F. Martenyi, S. M. Sheehan, L. N. Boggs, S. A. Monk, B. M. Mathes, D. J. Mergott, B. M. Watson, S. L. Stout, D. E. Timm, E. Smith Labell, C. R. Gonzales, M. Nakano, S. S. Jhee, M. Yen, L. Ereshefsky, T. D. Lindstrom, D. O. Calligaro, P. J. Cocke, D. Greg Hall, S. Friedrich, M. Citron, J. E. Audia, Robust central reduction of amyloid-β in humans with an orally available, non-peptidic β-secretase inhibitor. *J. Neurosci.* **31**, 16507–16516 (2011).
15. H. He, K. A. Lyons, X. Shen, Z. Yao, K. Bleasby, G. Chan, M. Hafey, X. Li, S. Xu, G. M. Salituro, L. H. Cohen, W. Tang, Utility of unbound plasma drug levels and P-glycoprotein transport data in prediction of central nervous system exposure. *Xenobiotica* **39**, 687–693 (2009).
16. J. A. Dobrowolska, M. S. Michener, G. Wu, B. W. Patterson, R. Chott, V. Ovod, Y. Pyatkivskyy, K. R. Wildsmith, T. Kasten, P. Mathers, M. Dancho, C. Lennox, B. E. Smith, D. Gilberto, D. McLoughlin, D. J. Holder, A. W. Stamford, K. E. Yarasheski, M. E. Kennedy, M. J. Savage, R. J. Bateman, CNS amyloid-β, soluble APP-α and -β kinetics during BACE inhibition. *J. Neurosci.* **34**, 8336–8346 (2014).
17. M. Willem, A. N. Garratt, B. Novak, M. Citron, S. Kaufmann, A. Rittger, B. DeStrooper, P. Saftig, C. Birchmeier, C. Haass, Control of peripheral nerve myelination by the β-secretase BACE1. *Science* **314**, 664–666 (2006).
18. X. Hu, C. W. Hicks, W. He, P. Wong, W. B. Macklin, B. D. Trapp, R. Yan, Bace1 modulates myelination in the central and peripheral nervous system. *Nat. Neurosci.* **9**, 1520–1525 (2006).
19. D. Esterházy, I. Stützer, H. Wang, M. P. Rechsteiner, J. Beauchamp, H. Döbeli, H. Hilpert, H. Matile, M. Prummer, A. Schmidt, N. Lieske, B. Boehm, L. Marselli, D. Bosco, J. Kerr-Conte, R. Aebersold, G. A. Spinas, H. Moch, C. Migliorini, M. Stoffel, Bace2 is a β cell-enriched protease that regulates pancreatic β cell function and mass. *Cell Metab.* **14**, 365–377 (2011).
20. D. R. Shimshek, L. H. Jacobson, C. Kolly, N. Zamurovic, K. K. Balavenkatraman, L. Morawiec, R. Kreutzer, J. Schelle, M. Jucker, B. Bertschi, D. Theil, A. Heier, K. Bigot, K. Beltz, R. Machauer, I. Brzak, L. Perrot, U. Neumann, Pharmacological BACE1 and BACE2 inhibition induces hair depigmentation by inhibiting PMEL17 processing in mice. *Sci. Rep.* **6**, 21917 (2016).
21. L. Rochin, I. Hurbain, L. Serneels, C. Fort, B. Watt, P. Leblanc, M. S. Marks, B. De Strooper, G. Raposo, G. van Niel, BACE2 processes PMEL to form the melanosome amyloid matrix in pigment cells. *Proc. Natl. Acad. Sci. U.S.A.* **110**, 10658–10663 (2013).
22. L. A. Hyde, C. Cantù, B. Werner, X. Chen, M. Sondey, M. Chen, B. Weig, A. LaShomb, X. Lu, R. A. Hodgson, J. Scott, J. Cumming, A. Stamford, E. M. Parker, M. E. Kennedy, Chronic BACE inhibition halts further age-related increases in brain Aβ and amyloid plaques in aged TgCRND8 mice with established plaques. *Alzheimer's Dementia* **8**, P188 (2012).
23. R. J. Bateman, G. Wen, J. C. Morris, D. M. Holtzman, Fluctuations of CSF amyloid-beta levels: Implications for a diagnostic and therapeutic biomarker. *Neurology* **68**, 666–669 (2007).
24. E. Karran, J. Hardy, A critique of the drug discovery and phase 3 clinical programs targeting the amyloid hypothesis for Alzheimer disease. *Ann. Neurol.* **76**, 185–205 (2014).
25. E. M. T. van Maanen, T. J. van Steeg, M. S. Michener, M. J. Savage, M. E. Kennedy, H. J. Kleijn, J. A. Stone, M. Danhof, Systems pharmacology analysis of the amyloid cascade following β-secretase inhibition enables the identification of an Aβ42 oligomer pool. *J. Pharmacol. Exp. Ther.* **357**, 205–216 (2016).
26. M. A. Willem, S. Tahirovic, M. A. Busche, S. V. Ovsepian, M. Chafai, S. Kootar, D. Hornburg, L. D. B. Evans, S. Moore, A. Daria, H. Hampel, V. Müller, C. Giudici, B. Nuscher, A. Wenninger-Weinzier, E. Kremmer, M. T. Heneka, D. R. Thal, V. Giedraitis, L. Lannfelt, U. Müller, F. J. Livesey, F. Meissner, J. Herms, A. Konnerth, H. Marie, C. Haass, η-Secretase processing of APP inhibits neuronal activity in the hippocampus. *Nature* **15**, 443–447 (2015).
27. Y. Mitani, J. Yarimizu, K. Saita, H. Uchino, H. Akashiba, Y. Shitaka, K. Ni, N. Matsuoka, Differential effects between γ-secretase inhibitors and modulators on cognitive function in amyloid precursor protein-transgenic and nontransgenic mice. *J. Neurosci.* **32**, 2037–2050 (2012).
28. J. Zhao, Y. Fu, M. Yasvoina, P. Shao, B. Hitt, T. O'Connor, S. Logan, E. Maus, M. Citron, R. Berry, L. Binder, R. Vassar, β-site amyloid precursor protein cleaving enzyme 1 levels become elevated in neurons around amyloid plaques: Implications for Alzheimer's disease pathogenesis. *J. Neurosci.* **27**, 3639–3649 (2007).
29. S. Barão, A. Gartner, E. Leyva-Díaz, G. Demyanenko, S. Munck, T. Vanhoutvin, L. Zhou, M. Schachner, G. López-Bendito, P. F. Maness, B. De Strooper, Antagonistic effects of BACE1 and APH1B-γ-secretase control axonal guidance by regulating growth cone collapse. *Cell Rep.* **12**, 1367–1376 (2015).
30. N. Mattsson, L. Rajendran, H. Zetterberg, M. Gustavsson, U. Andreasson, M. Olsson, G. Brinkmalm, J. Lundkvist, L. H. Jacobson, L. Perrot, U. Neumann, H. Borghys, M. Mercken, D. Dhuyvetter, F. Jeppsson, K. Blennow, E. Portelius, BACE1 inhibition induces a specific cerebrospinal fluid β-amyloid pattern that identifies drug effects in the central nervous system. *PLOS ONE* **7**, e31084 (2012).
31. P. C. May, B. A. Willis, S. L. Lowe, R. A. Dean, S. A. Monk, P. J. Cocke, J. E. Audia, L. N. Boggs, A. R. Borders, R. A. Brier, D. O. Calligaro, T. A. Day, L. Ereshefsky, J. A. Erickson, H. Gevorkyan, C. R. Gonzales, D. E. James, S. S. Jhee, S. F. Komjathy, L. Li, T. D. Lindstrom, B. M. Mathes, F. Martényi, S. M. Sheehan, S. L. Stout, D. E. Timm, G. M. Vaught, B. M. Watson, L. L. Winneroski, Z. Yang, D. J. Mergott, The potent BACE1 inhibitor LY2886721 elicits robust central Aβ pharmacodynamic responses in mice, dogs, and humans. *J. Neurosci.* **35**, 1199–1210 (2015).
32. J. Cai, X. Qi, N. Kociok, S. Skosyrski, A. Emilio, Q. Ruan, S. Han, L. Liu, Z. Chen, C. Bowes Rickman, T. Golde, M. B. Grant, P. Saftig, L. Serneels, B. de Strooper, A. M. Joussen, M. E. Boulton, β-Secretase (BACE1) inhibition causes retinal pathology by vascular dysregulation and accumulation of age pigment. *EMBO Mol. Med.* **4**, 980–991 (2012).
33. X. Hu, X. Zhou, W. He, J. Yang, W. Xiong, P. Wong, C. G. Wilson, R. Yan, BACE1 deficiency causes altered neuronal activity and neurodegeneration. *J. Neurosci.* **30**, 8819–8829 (2010).
34. M. R. Fielden, J. Werner, J. A. Jamison, A. Coppi, D. Hickman, R. T. Dunn II, E. Trueblood, L. Zhou, C. A. Afshari, R. Lightfoot-Dunn, Retinal toxicity induced by a novel β-secretase inhibitor in the Sprague–Dawley rat. *Toxicol. Pathol.* **43**, 581–592 (2015).
35. A. M. Zuhl, C. E. Nolan, M. A. Brodney, S. Niessen, A. Atchison, C. Houle, D. A. Karanian, C. Ambroise, J. W. Brulet, E. M. Beck, S. D. Doran, B. T. O'Neill, C. W. Am Ende, C. Chang, K. F. Geoghegan, G. M. West, J. C. Judkins, X. Hou, D. R. Riddell, D. S. Johnson, Chemoproteomic profiling reveals that cathepsin D off-target activity drives ocular toxicity of β-secretase inhibitors. *Nat. Commun.* **7**, 13042 (2016).
36. J. J. Shacka, B. J. Klocke, C. Young, M. Shibata, J. W. Olney, Y. Uchiyama, P. Saftig, K. A. Roth, Cathepsin D deficiency induces persistent neurodegeneration in the absence of Bax-dependent apoptosis. *J. Neurosci.* **27**, 2081–2090 (2007).
37. R. Vassar, P.-H. Kuhn, C. Haass, M. E. Kennedy, L. Rajendran, P. C. Wong, S. F. Lichtenthaler, Function, therapeutic potential and cell biology of BACE proteases: Current status and future prospects. *J. Neurochem.* **130**, 4–28 (2014).

38. K. Shirakabe,, S. Wakatsuki, T. Kurisaki, A. Fujisawa-Sehara, Roles of meltrin β/ADAM19 in the processing of neuregulin. *J. Biol. Chem.* **276**, 9352–9358 (2001).
39. B. De Strooper, L. Chávez Gutiérrez, Learning by failing: Ideas and concepts to tackle γ-secretases in Alzheimer's disease and beyond. *Annu. Rev. Pharmacol. Toxicol.* **55**, 419–437 (2015).
40. A. W. Stamford, J. D. Scott, S. W. Li, S. Babu, D. Tadesse, R. Hunter, Y. Wu, J. Misiaszek, J. N. Cumming, E. J. Gilbert, C. Huang, B. A. McKittrick, L. Hong, T. Guo, Z. Zhu, C. Strickland, P. Orth, J. H. Voigt, M. E. Kennedy, X. Chen, R. Kuvelkar, R. Hodgson, L. A. Hyde, K. Cox, L. Favreau, E. M. Parker, W. J. Greenlee, Discovery of an orally available, brain penetrant BACE1 inhibitor that affords robust CNS Aβ reduction. *ACS Med. Chem. Lett.* **3**, 897–902 (2012).
41. Z. Zhu, Z.-Y. Sun, Y. Ye, J. Voigt, C. Strickland, E. M. Smith, J. Cumming, L. Wang, J. Wong, Y.-S. Wang, D. F. Wyss, X. Chen, R. Kuvelkar, M. E. Kennedy, L. Favreau, E. Parker, B. A. McKittrick, A. Stamford, M. Czarniecki, W. Greenlee, J. C. Hunter, Discovery of cyclic acylguanidines as highly potent and selective β-site amyloid cleaving enzyme (BACE) inhibitors: Part I—Inhibitor design and validation. *J. Med. Chem.* **53**, 951–965 (2010).
42. M. Mandal, Y. Wu, J. Misiaszek, G. Li, A. Buevich, J. P. Caldwell, X. Liu, R. D. Mazzola, P. Orth, C. Strickland, J. Voigt, H. Wang, Z. Zhu, X. Chen, M. Grzelak, L. A. Hyde, R. Kuvelkar, P. Leach, G. Terracina, L. Zhang, Q. Zhang, M. Michener, B. Smith, K. Cox, D. Grotz, L. Favreau, K. Mitra, I. Kazakevich, B. A. McKittrick, W. Greenlee, M. E. Kennedy, E. M. Parker, J. N. Cumming, A. W. Stamford, Structure-based design of an iminoheterocyclic BACE1 inhibitor that lowers central Aβ in non-human primates. *J. Med. Chem.* **59**, 3231–3248 (2016).

Acknowledgments: We acknowledge the assistance of I. Kazakevich, P. Orth, C. Cantu, G. Wang, B. Werner, F. Eijnthoven, C. Canales, L. Ma, G. Krishna, M. Wirth, T. Forest, S. Kuruvilla, and O. Laterza (all from Merck & Co. Inc.) in performing one or more of the studies described in this paper. We also thank J. Luthman and J. Silber (Merck & Co. Inc.) for their oversight of the verubecestat early development program. The following primary investigators participated in the phase 1 clinical studies: J. Leempoels (Antwerp, Belgium; single-dose healthy nonelderly adult study), D. Han (Glendale, CA, USA; multiple-dose healthy nonelderly adult study), M. Bačkonja (Salt Lake City, UT, USA; multiple-dose AD patient study), H. Gevorkyan (Glendale, CA, USA; multiple-dose AD patient study), and J. Apter (Princeton, NJ, USA; multiple-dose AD patient study). C. Lines (Merck & Co. Inc.) assisted with the editing of the manuscript, and C. Strickland (Merck & Co. Inc.) assisted with Fig. 1. **Funding:** This work was funded by Merck & Co. Inc. (Kenilworth, NJ, USA). **Author contributions:** J.D.S., J.N.C., W.L., and A.W.S. performed the chemistry studies. M.E.K., R.K., X.C., R.A.H., and L.A.H. performed the animal biology and pharmacology studies. E.M.P., M.E.K., B.A.M., and L.A.H. contributed to the design and interpretation of the animal biology and pharmacology studies. K.C. and H.M. performed the animal PK/PD modeling work. M.D.T., J.L.T., M.T., J.P., and M.S.F. performed the human clinical pharmacology studies. L.E. and S.J. contributed to the design and conduct of the multiple-dose studies in healthy nonelderly adults and AD patients. M.F.D., H.J.K., and J.A.S. performed the human PK/PD modeling work. M.E. designed the phase 3 clinical trials. E.M.P., M.E.K., J.N.C., A.W.S., J.D.S., M.S.F., J.A.S., and M.E. wrote the paper with input from all the authors. **Competing interests:** All authors except L.E. and S.J. are current or former employees of Merck & Co. Inc. and own or owned stock/stock options in Merck & Co. Inc. L.E. and S.J. have received consulting fees from Merck & Co. Inc. The Patent Cooperation Treaty patent application WO 2011044181 "Iminothiadiazine dioxide compounds as BACE inhibitors and their preparation, compositions and use in the treatment of pathologies associated with beta-amyloid protein" covers verubecestat and pertains to the results presented in this paper. **Data and materials availability:** The clinical trial in AD patients described here is registered on ClinicalTrials.gov under the identifier NCT01496170. Detailed protocols for the clinical studies described in this manuscript are available in the Supplementary Materials. Verubecestat is currently being tested in two phase 3 clinical trials, which are also registered on ClinicalTrials.gov under the identifiers NCT01739348 and NCT01953601. The coordinates of the verubecestat/BACE1 crystal structure are deposited in the Protein Data Bank under the accession number 5HU1.

Submitted 1 March 2016
Accepted 14 October 2016
Published 2 November 2016
10.1126/scitranslmed.aad9704

Citation: M. E. Kennedy, A. W. Stamford, X. Chen, K. Cox, J. N. Cumming, M. F. Dockendorf, M. Egan, L. Ereshefsky, R. A. Hodgson, L. A. Hyde, S. Jhee, H. J. Kleijn, R. Kuvelkar, W. Li, B. A. Mattson, H. Mei, J. Palcza, J. D. Scott, M. Tanen, M. D. Troyer, J. L. Tseng, J. A. Stone, E. M. Parker, M. S. Forman, The BACE1 inhibitor verubecestat (MK-8931) reduces CNS β-amyloid in animal models and in Alzheimer's disease patients. *Sci. Transl. Med.* **8**, 363ra150 (2016).

Science Translational Medicine
AAAS

The BACE1 inhibitor verubecestat (MK-8931) reduces CNS β -amyloid in animal models and in Alzheimer's disease patients

Matthew E. Kennedy, Andrew W. Stamford, Xia Chen, Kathleen Cox, Jared N. Cumming, Marissa F. Dockendorf, Michael Egan, Larry Ereshefsky, Robert A. Hodgson, Lynn A. Hyde, Stanford Jhee, Huub J. Kleijn, Reshma Kuvelkar, Wei Li, Britta A. Mattson, Hong Mei, John Palcza, Jack D. Scott, Michael Tanen, Matthew D. Troyer, Jack L. Tseng, Julie A. Stone, Eric M. Parker and Mark S. Forman (November 2, 2016)

Science Translational Medicine **8** (363), 363ra150. [doi: 10.1126/scitranslmed.aad9704]

Editor's Summary

Getting to first BACE

The discovery of BACE1 inhibitors that reduce β-amyloid peptides in Alzheimer's disease (AD) patients has been an encouraging development in the quest for a disease-modifying therapy. Kennedy and colleagues now report the discovery of verubecestat, a structurally unique, orally bioavailable small molecule that potently inhibits brain BACE1 activity resulting in a reduction in A β peptides in the cerebrospinal fluid of animals, healthy volunteers, and AD patients. No dose-limiting toxicities were observed in chronic animal toxicology studies or in phase 1 human studies, thus reducing safety concerns raised by previous reports of BACE inhibitors and BACE1 knockout mice.

Science Translational Medicine (print ISSN 1946-6234; online ISSN 1946-6242) is published weekly, except the last week in December, by the American Association for the Advancement of Science, 1200 New York Avenue, NW, Washington, DC 20005.